Structure, Vol. 9, 527–537, June, 2001, ©2001 Elsevier Science Ltd. All rights reserved. PII S0969-2126(01)00613-X

A Structural Genomics Approach to the Study of Quorum Sensing: Crystal Structures of Three LuxS Orthologs

Hal A. Lewis,[1] Eva Bric Furlong, Boris Laubert, Galina A. Eroshkina, Yelena Batiyenko, Jason M. Adams, Mark G. Bergseid, Curtis D. Marsh, Thomas S. Peat, Wendy E. Sanderson, J. Michael Sauder, and Sean G. Buchanan
Structural GenomiX
San Diego, California 92121
USA

Summary

Background: Quorum sensing is the mechanism by which bacteria control gene expression in response to cell density. Two major quorum-sensing systems have been identified, system 1 and system 2, each with a characteristic signaling molecule (autoinducer-1, or AI-1, in the case of system 1, and AI-2 in system 2). The *luxS* gene is required for the AI-2 system of quorum sensing. LuxS and AI-2 have been described in both Gram-negative and Gram-positive bacterial species and have been shown to be involved in the expression of virulence genes in several pathogens.

Results: The structure of the LuxS protein from three different bacterial species with resolutions ranging from 1.8 Å to 2.4 Å has been solved using an X-ray crystallographic structural genomics approach. The structure of LuxS reported here is seen to have a new alpha-beta fold. In all structures, an equivalent homodimer is observed. A metal ion identified as zinc was seen bound to a Cys-His-His triad. Methionine was found bound to the protein near the metal and at the dimer interface.

Conclusions: These structures provide support for a hypothesis that explains the in vivo action of LuxS. Specifically, acting as a homodimer, the protein binds a methionine analog, S-ribosylhomocysteine (SRH). The zinc atom is in position to cleave the ribose ring in a step along the synthesis pathway of AI-2.

Introduction

Quorum sensing, which can be defined as the signaling of cell density cues, is a widespread system of intercellular communication among bacteria. By monitoring the local density of cells of the same or different species, bacteria can respond by altering gene expression and, ultimately, behavior to best exploit the new circumstances. Quorum sensing is critical for the virulence of many bacteria that pose significant medical and agricultural threats. For example, *Pseudomonas aeruginosa* can be life threatening to cystic fibrosis patients because it forms multicellular aggregates (biofilms) that are highly resistant to most antibiotics, and biofilm development depends on quorum-sensing pathways [1]. In addition, certain crop pests, for example, *Erwinia carotovora, Ralstonia solanacearum*, and *Agrobacterium tumefaciens* (see [2] for a review) require an intact quorum-sensing pathway for pathogenicity. The quorum-sensing pathway is therefore an attractive target for the development of novel antibacterial agents. Indeed, many plants [3, 4] and bacteria [5] have evolved mechanisms to disrupt the quorum-sensing pathway of their predators.

Quorum sensing has been studied in marine *Vibrio* species in which bioluminescence is stimulated at high cell density [6]. For example, *Vibrio harveyi* utilizes two classes of signaling molecule or autoinducer, AI-1 and AI-2. AI-1 has been characterized from several species of Gram-negative bacteria as being various acylated derivatives of homoserine lactone (HSL). Three distinct families of acyl-HSL synthase have been characterized that are not obviously related at the sequence level. These are the LuxI family, the LuxM/AinS family [7], and the HdtS family [8]. Quorum sensing by AI-2 appears to be more widespread, having been identified in both Gram-positive and Gram-negative species. AI-2 production depends on the proper function of the *luxS* gene [9]. The LuxS protein is unrelated to any of the acyl-HSL synthase families and its specific biochemical function in AI-2 biosynthesis is unclear. AI-2 is unlikely to be an acyl-HSL, as it cannot be isolated using techniques that purify this class of compounds [9, 10]. A recent patent (Bassler, B., 2000, Patent WO 00/32152) indicates that the identity of AI-2 is 4,5-dihydroxy-2-3-pentanedione.

Structural genomics is an emerging field of postgenomic discovery (see supplement to Nature Structural Biology, November, 2000). With the development of high-throughput structure determination methodologies, structural biology is poised to have a more pervasive influence than ever. In particular, protein structure will aid the assignment of biochemical function to the large fraction of genomes of unknown function. Whereas, classically, the X-ray crystallographer might target a single protein of particular interest, with the improvements in efficiency, it is possible to undertake structural studies of entire protein families or protein pathways. Several representative structures within a family highlight similarities and differences between family members. This information can help distinguish artifacts of the crystallization process from biologically meaningful results and help identify important functional residues that are conserved in both sequence and space. Structures of several family members are of special value to the medicinal chemist attempting to design selective compounds with reduced side effects or, conversely, broad spectrum antimicrobial agents.

In our structural genomics efforts, we have combined the pathway and family approaches to understand the mechanisms of quorum sensing in molecular detail. Our

[1]Correspondence: hal_lewis@stromix.com

Key words: autoinducer-2; LuxS; quorum sensing; structural genomics

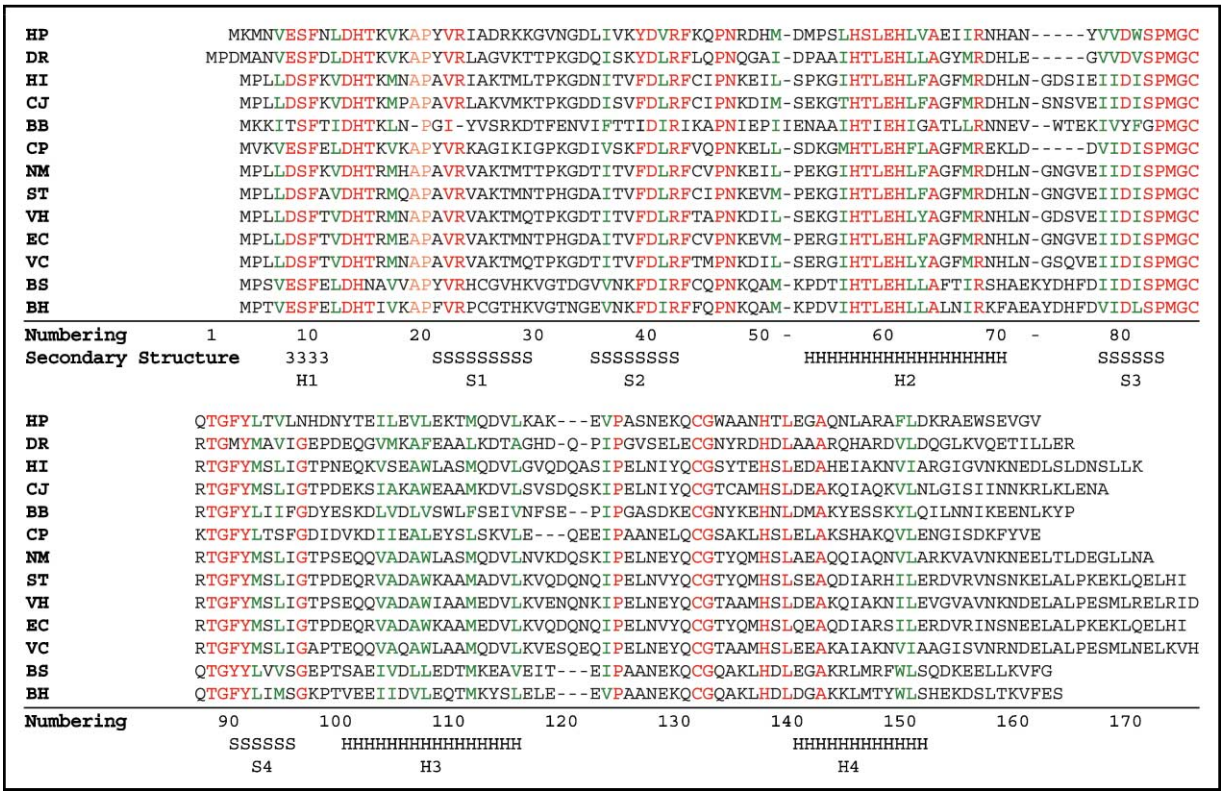

Figure 1. Sequence Alignment of Some LuxS Proteins

Color coding: red indicates greater than 92% identity (or homology, in the case of Phe/Tyr, Ser/Thr, and Asp/Glu), and green indicates hydrophobic side chain conservation. The residue numbering employed in the text as well as the principal LuxS secondary structure as determined in this study with 3 = 3_{10} helix, S = β strand, and H = α helix is indicated at the bottom. Proteins used in the sequence alignment are as follows (Protein Information Resource database ID numbers are shown in parentheses, with GenBank ID numbers given for ST, VH, and BH): HP, *Helicobacter pylori* (C71973); DR, *Deinococcus radiodurans* (D75280); HI, *Haemophilus influenzae* (G64008); CJ, *Campylobacter jejuni* (H81325); BB, *Borrelia burgdorferi* (BB0377); CP, *Clostridium perfringens* (T43793); NM, *Neisseria meningitidis* (G81963); ST, *Salmonella typhimurium* (AAF73475.1); VH, *Vibrio harveyi* (AAD17292.1); EC, *Escherichia coli* (H65048); VC, *Vibrio cholerae* (F82309); BS, *Bacillus subtillis* (A69994); and BH, *Bacillus halodurans* (BAB07072.1).

strategy is to attempt, in parallel, the cloning, expression, purification, and crystallization of multiple orthologs of each component on the pathway. Here, we describe the structure of one component of the AI-2 biosynthesis pathway, LuxS, from three different bacteria, *Helicobacter pylori*, *Deinococcus radiodurans*, and *Haemophilus influenzae*. The three structures allow us to characterize LuxS as a metalloenzyme, identify the active site residues, and suggest the likely mechanism for the reaction.

Results

Structure Determination

LuxS from five different bacteria were selected as part of our structural genomics effort [11]. As there is little published biochemical information about LuxS, it was expected that determining the structure of the protein would lead to new functional insights. Expressing, purifying, and crystallizing a protein from many different organisms improves the chance of successfully obtaining a structure. Furthermore, multiple structures within a family add confidence to functional interpretations and illuminate the regions of variability and conservation that may be of interest in protein engineering and small molecule design and in the understanding of functional differences.

Figure 1 shows an alignment of 13 LuxS sequences. Residues with strong homologies are indicated by color (see legend of Figure 1). Five of these proteins (LuxS orthologs from *Helicobacter pylori*, *Deinococcus radiodurans*, *Haemophilus influenzae*, *Borrelia burgdorferi*, and *Campylobacter jejuni*) were selected for cloning, expression, and purification for crystallization studies. The work of Bassler (Patent WO 00/32152) describes AI-2 production capability for all five of these bacteria. The sequences were identical to those shown in Figure 1, with the exception of the addition of a histidine tag sequence, GSHHHHHH, at the C termini of each. The average, pairwise identity among these five sequences is 38%. This suggests a strong structural similarity between these proteins, which is confirmed by the X-ray crystallographic results described below.

Of the five LuxS proteins selected, four expressed and purified in sufficient quantities for crystallization trials, and three were successfully crystallized, each with different space groups and unit cell dimensions (see Experimental Procedures). These three LuxS proteins are from *H. pylori*, *D. radiodurans*, and *H. influenzae*. The LuxS protein from *D. radiodurans* crystallized in

Table 1. Data Collection and Refinement Statistics

LuxS MAD Data Collection

	Wavelength (Å)	Resolution (Å)	Completeness (%) Overall/Outer Shell	R_{sym} (%) Overall/Outer Shell	MAD F.O.M.
H. pylori	0.9795 (L1)	37.0–2.38	100.0/100.0	5.6/19.8	0.66
	0.9641 (L2)	37.0–2.38	100.0/100.0	5.5/26.0	
H. influenzae	0.9795 (L1)	32.0–2.10	99.6/98.6	6.4/18.4	0.68
	0.9641 (L2)	32.0–2.10	99.4/98.1	5.7/20.3	
D. radiodurans, space group $P2_1$	0.9795 (L1)	23.0–1.80	86.0/100.0	7.0/15.3	0.60
	0.9641 (L2)	23.0–1.80	85.6/99.2	5.8/19.6	

LuxS MR Data Collection

	Wavelength (Å)	Resolution (Å)	Completeness (%) Overall/Outer Shell	R_{sym} (%) Overall/Outer Shell	R	C.C.
D. radiodurans, C2 with methionine	0.9641	35.0–2.10	98.1/100.0	5.3/7.4	0.39	0.54
D. radiodurans, C2 with no methionine	1.5418	39.0–2.00	99.9/98.5	4.9/7.1	0.40	0.58

Refinement Statistics

	Resolution (Å)	R	R_{free}	Waters	Rmsd Bond Length (Å)	Rmsd Bond Angles (°)	Average B values (Å^2) (molA/molB)
H. pylori	35.0–2.38	0.219	0.264	21	0.009	1.5	34.9/33.7
H. influenzae	30.0–2.10	0.213	0.238	57	0.008	1.4	26.7/25.9
D. radiodurans, $P2_1$	20.0–1.80	0.206	0.240	120	0.009	1.5	18.0/18.5
D. radiodurans, C2 with methionine	35.0–2.10	0.196	0.243	46	0.007	1.4	18.6
D. radiodurans, C2 with no methionine	35.0–2.00	0.182	0.236	80	0.009	1.5	11.3

$R_{sym} = \Sigma_{hk}\Sigma_i |I_i(hkl) - \langle I(hkl)\rangle| / \Sigma_{hk}\Sigma_i I_i(hkl)$, where I_i is the intensity of the observation and $\langle I\rangle$ is the mean intensity of the reflection. F.O.M is the figure of merit $= \langle |\Sigma P(\alpha) e^{i\alpha} / \Sigma |P(\alpha)| \rangle$, where α is the phase and $P(\alpha)$ is the phase probability distribution. $R = \Sigma ||F_o| - |F_c|| / \Sigma |F_o|$, where F_o and F_c are the observed and calculated structure-factor amplitudes, respectively. R_{free} is the same as R, except calculated for 10% of the data randomly omitted from the refinement. C.C. is the correlation coefficient $= \langle (|F_o| - \langle |F_o| \rangle)(|F_c| - \langle |F_c| \rangle) \rangle / \mathrm{sqrt}[\langle (|F_o| - \langle |F_o| \rangle)^2 \rangle \langle (|F_c| - \langle |F_c| \rangle)^2 \rangle]$. Rmsd is root-mean-square deviation. Average B values are reported for all nonhydrogen atoms and are separated into A and B molecules in the asymmetric unit when appropriate.

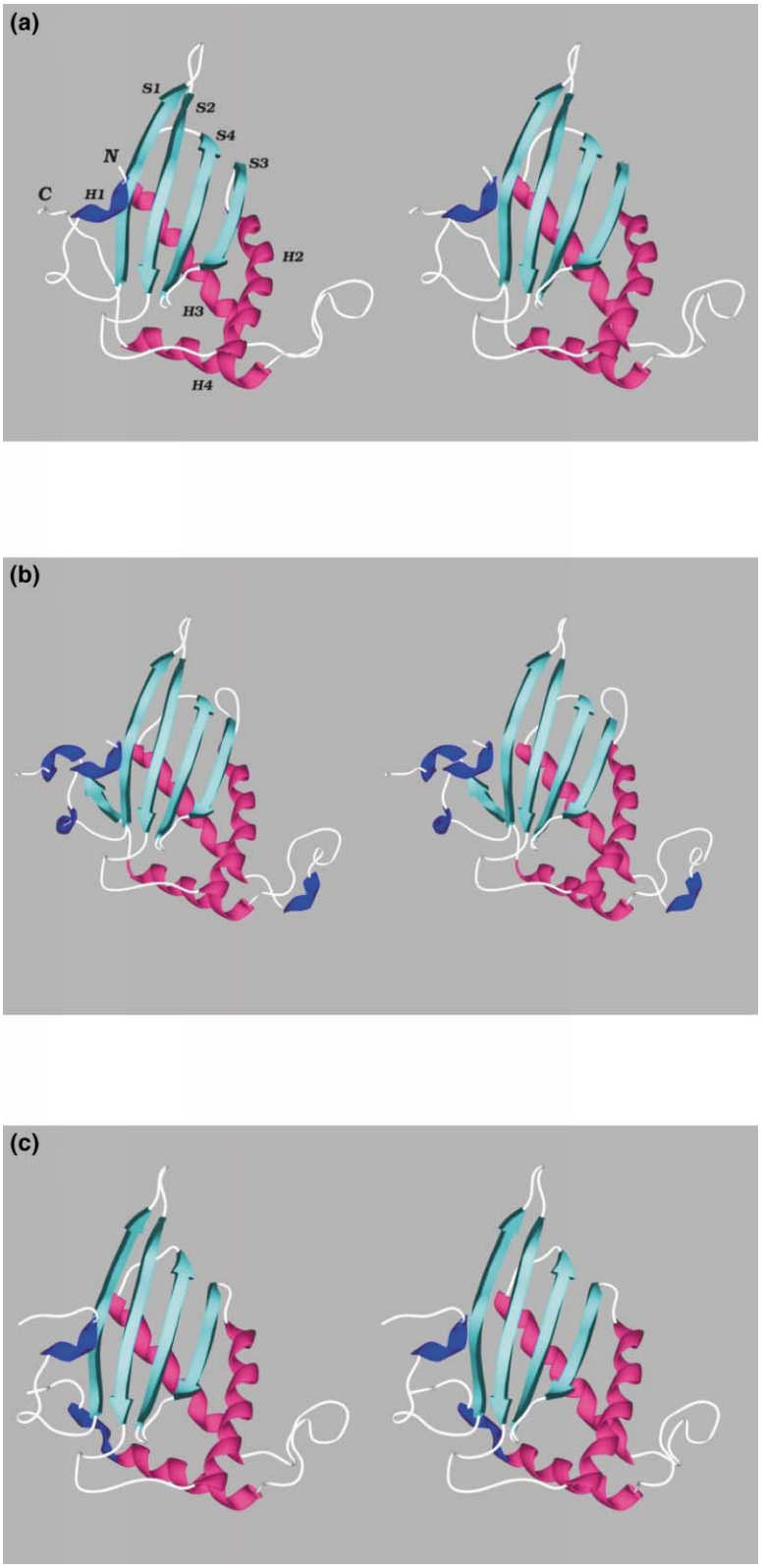

Figure 2. Stereo Ribbon Diagrams of One Monomer in the Asymmetric Unit of the LuxS Proteins Examined in This Paper

Beta strands are displayed in cyan, α helices are displayed in red, and 3_{10} helices are displayed in blue.

(a) LuxS from *H. pylori*. The N and C termini are indicated, as is the identity of the main secondary structural elements.

(b) LuxS from *H. influenza*.

(c) LuxS from *D. radiodurans*.

both of the two space groups, $P2_1$ and C2, giving yet another independent determination of the LuxS structure. Two *D. radiodurans* C2 structures were solved, one with methionine present in the crystallization conditions and one without, in order to observe any effect methionine binding might have on the LuxS fold. The LuxS structures obtained from all three organisms exhibited one dimer per asymmetric unit. Additionally, *D. radiodur-*

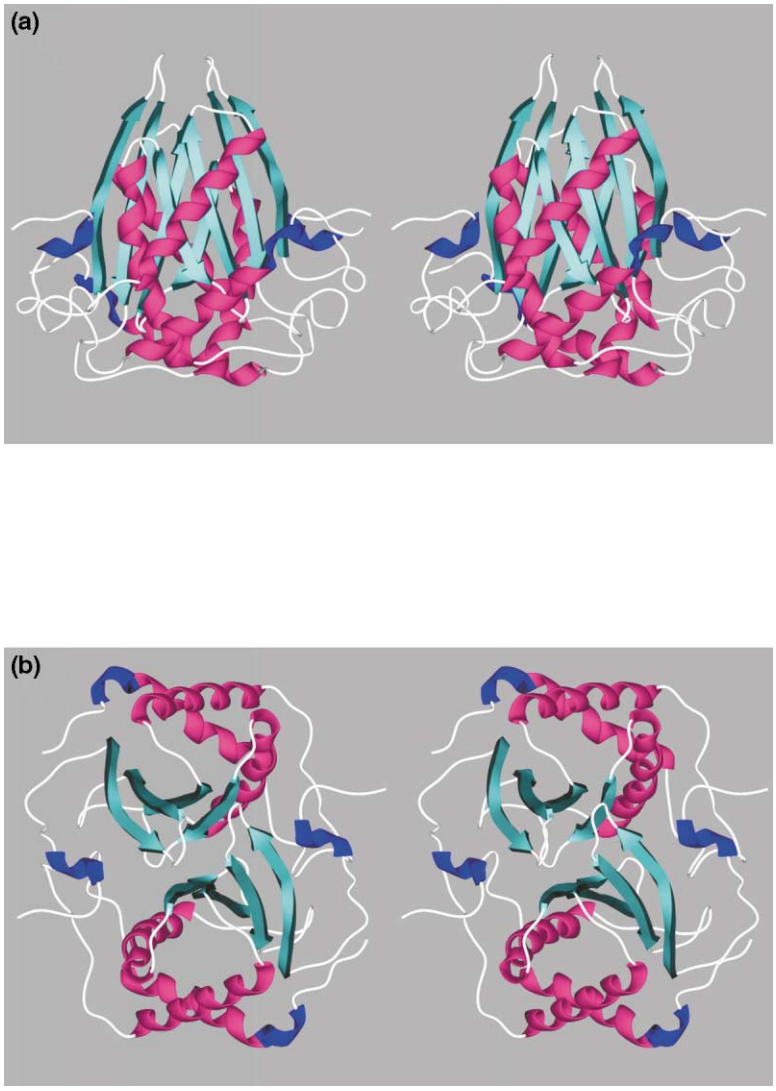

Figure 3. Stereo Ribbon Diagram of the LuxS Homodimer

The same color coding as that shown in Figure 2 is used.
(a) The dimer observed in the asymmetric unit of Hp_LuxS.
(b) Same as in (a), except rotated 90° out of the plane of the page.

ans crystals obtained in space group C2 displayed one monomer per asymmetric unit, forming a nearly identical dimer through crystallographic symmetry.

Table 1 describes the data used to determine the structures. Selenomethionine-labeled protein was produced for all three proteins, and crystals of these proteins were subjected to two wavelength (peak, L1; high energy, L2) multiwavelength anomalous diffraction (MAD) experiments. In the case of Hp_LuxS, 10 of the 12 Se atoms in the asymmetric unit were identified using Shake-and-Bake [12] and phased with SHARP [13]. Similarly, 12 of the 14 Se sites were found and used in the Hi_LuxS dataset, as were 11 of the 14 Se sites for Dr_LuxS. Excellent maps were obtained in each case after iterative solvent flattening using the Solomon algorithm [14].

Data were also collected for Dr_LuxS crystals possessing a different space group, C2, both with and without methionine present. The *D. radiodurans* LuxS structure obtained from the MAD dataset was used as a search model using the molecular replacement (MR) program EPMR [15]. R factors and correlation coefficients for the solutions reported by the program demonstrated the correctness of the solutions that were found (see Table 1).

The models produced from these maps were of very high quality (see "Average B values" in Table 1), excluding short spans of residues at the N and C termini. The Hp_LuxS model contained residues 3–160 (monomer A in the asymmetric unit) or 3–161 (monomer B). Residue numbering is as given in Figure 1. Similarly, the Hi_LuxS model covers residues 6–166 (A) or 6–165 (B), and the Dr_LuxS model spans residues 6–162 ($P2_1$ monomer A), 7–162 ($P2_1$ monomer B), 7–163 (C2 with methionine), and 7–164 (C2 without methionine). Residues in the histidine tag were not observed in any of the LuxS structures.

Structure of the LuxS Monomer

Figure 2 shows the arrangement of secondary structure elements from one representative monomer from each LuxS protein. The overall folds observed for LuxS are similar and consist of a four-stranded antiparallel β sheet in contact with four α helices. These are arranged in the order H1-S1-S2-H2-S3-S4-H3-H4 (see Figures 1 and 2). The primary differences between the three struc-

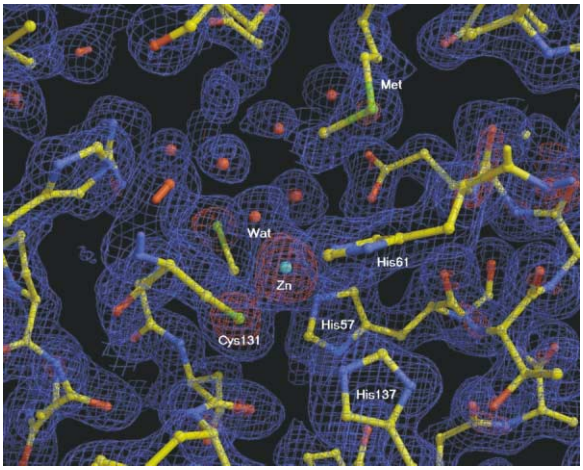

Figure 4. Experimental Map of Dr_LuxS Displaying Electron Density About the Metal Binding Site

The metal-coordinating side chains of His57, His61, and Cys131 are shown, as is the methionine ligand. A water molecule that coordinates directly with the metal is also indicated. Two color-coded density levels are shown; blue indicates 1σ, and red indicates 5σ. The figure was generated using XtalView [26].

tures reside in the N- and C-terminal regions. These include a 3_{10} α-helical extension of helix 4 in Hp_LuxS (residues 152–155) and three additional 3_{10} α helices in Hi_LuxS (at residues 14–16, 120–122, and 159–162) as well as a fifth strand in the fold's β sheet (residues 155–157). The superposition of the monomer from one protein onto the monomer of another was calculated (using C_α atoms from the core residues 11–70, 77–95, 101–117, and 125–151) and was found to average 0.93 Å rmsd (root-mean-square deviation), ranging from 0.78 Å for Dr_LuxS against Hi_LuxS to 1.08 Å for Hp_LuxS against Hi_LuxS, indicating a highly conserved fold between species. Except for somewhat greater flexibility at the termini and the loop connecting helices three and four, the overall structures are well ordered. Many of the conserved residues in the LuxS protein are hydrophobic in nature (green in Figure 1). It is clear from a plot of these conserved residues on the structure (data not shown) that the majority of the residues form the hydrophobic core of LuxS, between the β sheet and α helices 2–4.

The Protein Data Bank was explored using DALI [16] to identify similar folds. The best match was against a portion of the cytochrome bc1 complex, molecule B [17] (Dali z-score of 6.0, rmsd of aligned residues of 3.4 Å). Similarities with strands S1, S2, and S4 of LuxS are seen as well as helices H1–H4. However, a match with strand S3 is missing, two new helices are present, and the loop regions, particularly the important metal binding loop between H3 and H4, are completely different. It is clear that the LuxS fold is significantly different and, to the best of our knowledge, represents a new protein fold in the alpha-beta family.

Homodimer

All three proteins displayed a homodimer interaction in their asymmetric units. This is illustrated in Figure 3.

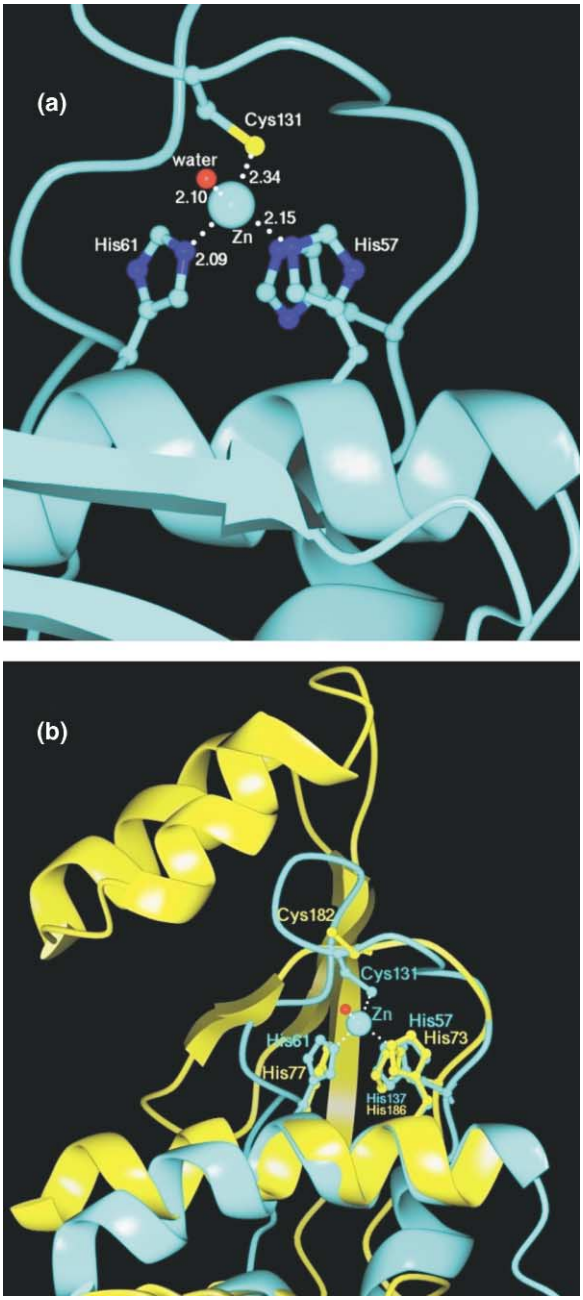

Figure 5. Ball and Stick and Ribbon Diagrams of the Metal Binding Site

(a) The metal binding pocket of Hp_LuxS with His61, His57, His137, and Cys131 side chains shown as a ball and stick. Interactions between the zinc ion and potential hydrogen bonding partners are indicated with dotted lines and distances in Å. The water molecule occupying the fourth coordination site of the zinc is also indicated. (b) The putative metal binding pocket from threonyl-tRNA synthetase (yellow) is superimposed on the LuxS zinc binding pocket (cyan) shown in (a).

This dimerization was highly consistent amongst the three structures (α carbon superpositions of the dimers ranging from 0.88 $Å^2$ for Dr_LuxS onto Hi_LuxS to 1.15 $Å^2$ for Dr_LuxS onto Hp_LuxS for residues 11–70, 77–95, 101–117, and 125–151 of each monomer). The surface

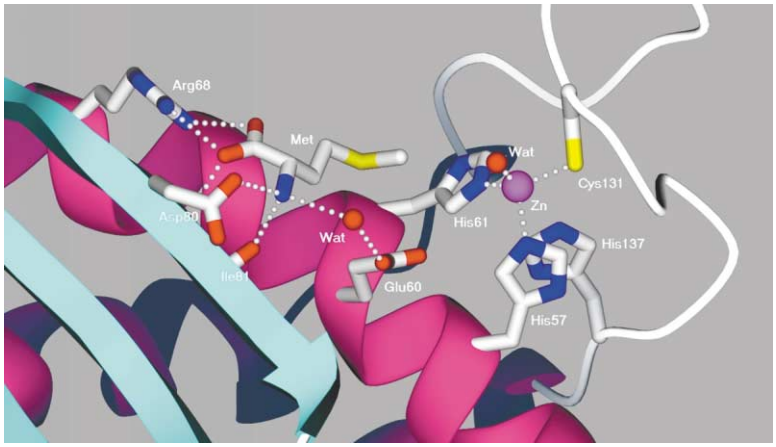

Figure 6. Ball and Stick and Ribbon Diagram of the Substrate and Metal Binding Sites

Potential hydrogen-bonding partners for the methionine ligand are shown by white dotted lines. Potential hydrogen bonding interactions with the zinc atom are also shown.

area buried through this interaction is considerable, comprising nearly a quarter of the entire surface of each monomer; 3930 Å^2 for Dr_LuxS, 4160 Å^2 for Hi_LuxS, and 4180 Å^2 for Hp_LuxS. In the case in which one molecule was seen in the asymmetric unit (C2 of Dr_LuxS), the same homodimer was seen through crystallographic symmetry. The metal and substrate binding sites also lie at the dimer interface (see below). Dynamic light-scattering studies [18] of all four soluble proteins showed a monodisperse dimer interaction in solutions of the LuxS proteins (apparent molecular weights of 1.8–2.1 times that of the monomer, data not shown). In combination, these data strongly support the conclusion that LuxS functions as a homodimer in solution.

Metal Binding Pocket

Analysis of the LuxS data revealed electron density in a binding pocket (Figure 4), composed of His57, His61, and Cys131 in coordination distance with a metal atom (2.6 Å or less) and with His137 nearby in a supporting role (vdW contacts of His137 with His57 is 3.3 Å [closest contact], with His61 is 3.8 Å [closest], and with Cys131 is 3.7 Å [closest]). Figure 5a shows this arrangement. The identity of the metal was subsequently established to be zinc, as demonstrated by EXAFS data measured on crystals at the Advanced Photon Source synchrotron (data not shown). The zinc is tetra-coordinated, with density likely representing a water molecule occupying the fourth coordination site. This is very suggestive of an enzymatic role for the metal, as many zinc enzymes have a similarly coordinated zinc ion [19].

The Dali search was repeated, this time using only helices 2,3, and 4 and the loop region between helices 3 and 4. This was done to search for structures with similar metal binding pockets to LuxS. One hit, the N2 domain of *E. coli* threonyl-tRNA synthetase (ThrRS) complexed with threonine tRNA [20] (Dali z-score of 3.6), displayed a similar arrangement of histidines and cysteine (Figure 5b). No metal ion was found by the authors of this study, and the cysteine thiol group was modeled as pointing away from the putative metal binding site. This domain is believed to perform the editing function, hydrolyzing incorrectly formed Ser-tRNA^{Thr} [21]. The authors point out that alanine-tRNA synthetase has a homologous domain of unknown function in its C terminus. In fact, using a sensitive sequence-based method (ISS, [22]), we can detect the relationship between the N2 domain of ThrRS and LuxS despite just 5% amino acid identity in the aligned region. The sequence alignment of LuxS with the two synthetases shows a strong correlation with the secondary structure in the first half of this region (data not shown). However, the synthetases have a large insert not seen in LuxS and possess different secondary structure in the C-terminal region. The superposition of the α carbons of just the three histidines and the cysteine in the binding site is 2.1 Å rmsd. When the superposition was extended to common residues from helix 2–helix 4 in LuxS, the rmsd value increased to 5.8 Å. Thus, the similarity in structure is not necessarily indicative of a common evolutionary origin (see Discussion).

Substrate Binding Site

After the modeling of the LuxS protein into the experimental electron density, an interesting patch of residual density near the metal binding site was observed. Methionine was present in the protein solution used for crystallization in 10 mM concentration, and the extra density was consistent with a bound methionine molecule (see Figures 4 and 6). This ligand was seen in both monomers in the asymmetric unit for Hp_LuxS and Hi_LuxS and in one of the space group $P2_1$ molecules (monomer B) in Dr_LuxS. There is no evidence that methionine plays an in vivo role as a substrate for LuxS. Indeed, the methionine side chain is too short to reach the metal site (see Figures 4 and 6).

The recognition of this bound amino acid is through its backbone atoms (see Figure 6). The carboxylate group is within hydrogen bonding distance of the Ile81 backbone amide proton (2.8 Å) and the guanidinium group of the Arg68 side chain (3.1 Å). The amino group of the methionine ligand is within hydrogen bonding distance of Ile81 backbone carbonyl group (2.8 Å) and the side chain carboxylate group of Asp80 (2.6 Å). A water-mediated hydrogen bond from the methionine amino group to the side chain carboxylate of Glu60 is also seen. Glu60, Arg68, and Asp80 are highly conserved in the LuxS proteins (see Figure 1), indicating that all possess this capacity to bind an amino acid or a modified amino acid.

Van der Waal contacts of the methionine are made

with both molecules in the homodimer. The closest approaches to the methionine side chain from nearby side chain atoms are: 3.3 Å for Asp80, 3.9 Å for Glu60, 3.8 Å for Ala64, and 3.8 Å for His61, which are all in the monomer that is binding the methionine backbone; and 3.8 Å for Tyr91, 3.6 Å for Ser9, 3.3 Å for Phe10, and 3.5 Å for Leu7, all from the other molecule in the homodimer. The significance of these contacts is emphasized by the fact that all but Leu7 are highly conserved in the LuxS motif (see Figure 1).

Crystals of Dr_LuxS, space group C2, were obtained using protein that had not been exposed to 10 mM methionine, unlike the other protein samples. The structure was determined using molecular replacement and, as expected, showed no methionine in the substrate binding site. The structure was essentially identical to that seen with methionine present. This means that the overall fold of LuxS is independent of methionine (and presumably substrate) binding and that the homodimer structure (seen as a crystallographic dimer in the C2 data) is unaltered upon Met binding.

Discussion

The structures of three LuxS orthologs provide a new understanding of the AI-2 biosynthesis pathway and the likely role of LuxS. LuxS has a zinc binding site comprised of two histidines and a cysteine, suggesting that the protein is a zinc metalloenzyme, the protein is a homodimer in solution, and observations of a bound methionine supports arguments that the LuxS substrate is an amino acid derivative.

Evidence for the importance of the homodimer in the function of LuxS is that the methionine ligand binding occurs at the dimer interface (see Figure 7a). Additionally, channels in the protein that lead to and from the substrate binding site, providing access for substrate and egress for product, are visible. One channel leads through one monomer to the binding site of the other. Yet, more evidence of the importance of the homodimer is apparent from plots of electrostatic potential on the monomer surfaces (Figure 7b) and plots of residue conservation (Figures 7c). It is clear from Figure 7b that there is a charge complementarity to the surfaces that interact to form the dimer. Also, Figure 7c demonstrates that the majority of conserved, nonhydrophobic residues line the dimerization domain, which is also the metal and amino acid binding domains, emphasizing its importance.

The methionine present in the structures is an artifact of the purification procedure, since it was not present in protein purified in the absence of this reagent (10 mM methionine is added as an oxidative sink as part of our standard protein handling protocol). However, the methionine backbone interactions with highly conserved residues in LuxS indicate that the physiological substrate is an amino acid or a derivative thereof. In fact, many signals used by bacteria for intercellular communication are amino acid based. Additionally, Bassler has claimed (Patent WO 00/32152) that the LuxS substrate is S-ribosylhomocysteine. In our modeling studies, we found that S-ribosylhomocysteine fits well into this site (see Figure 8). The methionine ligand observed from the electron density is a good model for the homocysteine portion of SRH, being an exact match from the amino acid backbone to the C5′ carbon atom. By adjusting the position of the ribosyl portion of SRH, hydrogen bonding contacts can potentially be formed between the zinc and O4′ of the ribose ring, between

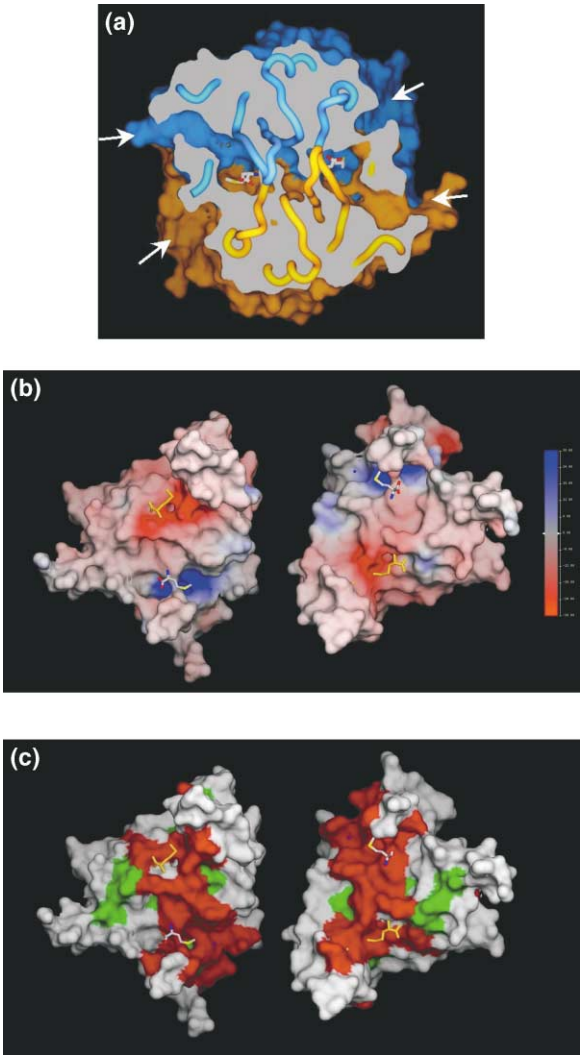

Figure 7. Molecular Surface Representations of the LuxS Homodimer

(a) A diagram of the surfaces of the two molecules in the asymmetric unit of Hi_LuxS (one blue and one gold), partially cut away to reveal bound methionine (ball and stick representations) and channels leading to and from the substrate binding site (indicated by arrows). Worm representations of the protein backbone atoms in the cutaway region are also shown.

(b) A surface diagram of the Hi_LuxS homodimer, with the monomers separated and rotated toward the viewer. The methionine ligands are represented as a ball and stick, one per monomer, with virtual ligands representing where the methionine would lay across the opposing molecule shown in gold. Red represents negative potential, and blue represents positive potential, covering the range from −30 kT to +30 kT.

(c) A similar surface diagram representation to that in (b), except green and red coloring indicate the position of conserved residues in the LuxS family (same color coding as in Figure 1).

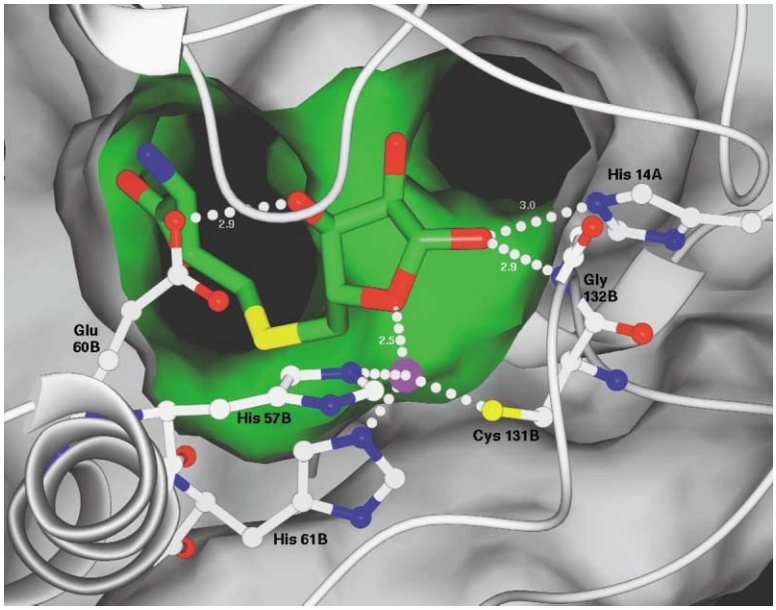

Figure 8. Modeling of S-ribosylhomocysteine into the Ligand Binding Pocket of One Monomer of Dr_LuxS

The zinc atom is indicated in purple. Likely hydrogen bond donor and acceptor interactions are indicated by dotted lines, with distance in Å. Channels in the protein that lead to and from the substrate, providing egress for substrate and product, are visible.

O1′ of the ring and NE2 of His14 and the backbone nitrogen of Gly132, and between O3′ of the ring and OE1 of Glu60.

Miller and Duerre performed work in 1968 [23] that seems to have relevance to this study. They describe an enzyme with characteristics strikingly similar to those hypothesized for LuxS, in that both enzymes hydrolyze S-ribosylhomocysteine to homocysteine plus another unidentified product. The authors of this work were only able to characterize the second product as being derived from the ribose moiety of SRH. This is reminiscent of the difficulty contemporary researchers have experienced in determining the identity of AI-2. Our studies are clearly consistent with this scheme. We propose that LuxS is the same enzyme described in the older work and that the LuxS structure is consistent with AI-2 production that is dependent upon the processing of SRH. From the structure of LuxS reported here, it seems probable that the sugar ring of SRH is cleaved by the zinc ion. This could lead to the production of the AI-2 signaling molecule directly or through subsequent processing by another enzyme. SRH is in fact derived from SAM (S-adenosylmethionine). It is interesting, therefore, that both AI-1 and AI-2 production may utilize a common precursor. Signal production in either system may become abrogated in nutrient-deprived cells in which there is competition for a limited amount of substrate.

By using a structural genomics approach, we have been able to unambiguously model the structure of LuxS and identify important characteristics of this enzyme. Further studies are needed to confirm the identity of the substrate and product as well as the specific function of LuxS in the catalytic reaction. In particular, SRH is being prepared enzymatically in our labs with the intent of performing cocrystallization experiments to demonstrate the exact binding mechanism of this substrate. This will also allow enzymatic assays to be performed to compare the activities of various LuxS proteins. In summary, the structures presented here will greatly aid subsequent research into the biology of quorum-sensing signaling system 2.

Biological Implications

Quorum sensing is employed by bacteria to detect the presence and number of other bacteria in their environment, and a bacterium responds to this information by altering patterns of gene expression. Many pathogens do not express virulence factors before reaching high density, presumably to avoid alerting the host until the bacteria numbers are large enough to overcome an immune response. Therefore, quorum-sensing pathways represent a novel point of intervention for the development of antibiotics. One quorum-sensing pathway, signaling system 2, is utilized by a wide variety of bacteria and appears to be a nonself-specific method of sensing environmental cell density. This system may provide a target for novel broad-spectrum antibacterial agents.

System 2 is relatively poorly understood. From genetic studies, LuxS is known to be required for AI-2 generation but its specific biochemical role is unclear, and no other components of the AI-2 biosynthesis pathway have been described. This paper reports the structure of the LuxS protein from three bacterial species. The three structures assume a novel fold and reveal that LuxS is a zinc enzyme that likely acts as a homodimer. The substrate binding site, near the zinc site, is observed through binding of the substrate analog methionine. These structures provide confirming evidence to Bassler's work (Patent WO 00/32152) that the natural substrate for LuxS is an amino acid derivative and the chemical mechanism for AI-2 synthesis involves cleavage of the ribosyl ring of SRH by zinc. Finally, there is an intriguing similarity between the LuxS active site and the editing domain of threonyl-tRNA synthetase that may provide clues to the catalytic mechanisms of both proteins.

Sites of metal binding, substrate binding, and homodi-

mer interaction are identified. These provide the groundwork for mutagenesis experiments to confirm the proposed catalytic action of LuxS. Also, drug candidates can now be explored that will interfere with AI-2 production and act as a multispecies antibiotic.

Experimental Procedures

LuxS from *H. pylori, D. radiodurans*, *H. influenzae, B. burgdorferi,* and *C. jejuni* were expressed, after induction with IPTG, as C-terminal His-tagged proteins in pET26b-derived expression vectors. All but *B. burgdorferi* resulted in soluble protein in sufficient yield to proceed to protein purification. Cells were sonicated, followed by protein isolation on a nickel-charged Pharmacia HiTrap chelating column and then gel filtration with a Pharmacia HiLoad 16/60 Superdex75 column. The samples were then concentrated to 5–160 mg/ml in 150 mM NaCl, 10 mM methionine, 1 mM β-mercaptoethanol, 10 mM HEPES (pH 7.5) buffer. A proprietary crystallization screen was employed to identify crystallization conditions in 96-well hanging drop trays. We were unable to obtain crystals from the *C. jejuni* LuxS protein, perhaps in part because of its very high solubility (160 mg/ml). Crystals were successfully obtained for the remaining three proteins. Including the additional eight residues (GSHHHHHH) on their C termini, the *H. pylori* construct was 160 residues in length, the *D. radiodurans* was 166 residues in length, and the *H. influenzae* was 175 residues in length. The His-tagged region was not removed prior to crystallization.

Crystal conditions for *H. pylori* LuxS were 32% PEG 1000, 200 mM ammonium sulfate, 100 mM MES (pH 5.75), 30 mM β mercaptoethanol (BME) per well, 20°C, 5 mg/ml protein concentration. After a few days–week, long spike-shaped crystals would appear. These diffracted to better than 2.4 Å resolution and possessed a tetragonal space group symmetry ($P4_12_12$, with a = b = 71.10 Å, β = 130.13°).

Crystallization conditions for *D. radiodurans* LuxS were 26% PEG MME 5000, 100 mM MES (pH 6.5), 30 mM BME per well, 4°C, 19 mg/ml protein concentration. Block-shaped crystals would appear overnight. These diffracted to better than 2.1 Å resolution and possessed one of two monoclinic space groups ($P2_1$, with a = 43.71 Å, b = 82.18 Å, c = 49.48 Å, and β =102.78°, and C2, with a = 51.19 Å, b = 70.14 Å, c = 49.73 Å, and β = 112.03°).

Crystallization conditions for *H. influenzae* LuxS were 21% PEG MME 5000, 100 mM Bis-Tris (pH 6.25), 30 mM BME per well, 12°C, 10 mg/ml protein concentration. After three days, rod-shaped crystals would appear. These diffracted to better than 2.1 Å resolution and possessed a tetragonal space group ($P4_22_12$, with a = b = 129.59 Å, c = 53.74 Å).

There are six methionines in the *H. pylori* construct and seven each in the *D. radiodurans* and *H. influenzae* constructs, providing an adequate number for MAD phasing analysis. Protein that incorporated selenomethionine was made. Crystals were generated and cryofrozen in 80% well solution plus 10% glycerol and 10% ethylene glycol (soaked for 30–60 s). Two wavelength MAD datasets (peak at 0.9795 Å, high energy at 0.9641 Å) were collected for each protein at the APS COM-CAT beamline. One degree oscillation data were collected in each case, with a total of 180° for *H. pylori*, 360° for *D. radiodurans*, and 185° for *H. influenzae*, with 1–2 s exposures. Data was collected using a MAR CCD detector. A dataset from crystals of *D. radiodurans* LuxS with no methionine in the crystallization buffer was collected on a Rigaku X-ray generator with MSC Raxis IV++ image plate detector, 10 min exposures using 1.5° oscillations.

The data were indexed and scaled using Denzo and Scalepack [24]. The selenium sites were identified using Shake-n-Bake [12]. These were subsequently refined, and phase information was obtained using SHARP [13]. Solvent flattening was employed using the Solomon routine in the SHARP interface. Solvent content (35%) was used for *H. pylori*, 50% was used for *H. influenzae*, and 44% was used for *D. radiodurans*. Excellent maps were obtained, and models were built using O [25] and XtalView [26]. CNX [27] was employed to refine the models. Figures were produced using SPOCK [28], except when otherwise noted.

Acknowledgments

We thank Kevin D'Amico for his help in running the COM-CAT beamline at the Advanced Photon Source. We also wish to thank Jon Christopher, Janet Newman, Eric de La Fortelle, Doug Livingston, Ketan Gajiwala, Jochen Muller-Dieckmann, Chris Lima, Sean McCarthy, Wayne Hendrickson, and Tim Harris for their comments on the manuscript.

Received: February 7, 2001
Revised: May 10, 2001
Accepted: May 10, 2001

References

1. Singh, P.K., Schaefer, A.L., Parsek, M.R., Moninger, T.O., Welsh, M.J., and Greenberg, E.P. (2000). Quorum-sensing signals indicate that cystic fibrosis lungs are infected with bacterial biofilms. Nature *407*, 762–764.
2. Bassler, B.L. (1999). How bacteria talk to each other: regulation of gene expression by quorum sensing. Curr. Opin. Microbiol. *2*, 582–587.
3. Rice, S.A., Givskov, M., Steinberg, P., and Kjelleberg, S. (1999). Bacterial signals and antagonists: the interaction between bacteria and higher organisms. J. Mol. Microbiol. Biotechnol. *1*, 23–31.
4. Teplitski, M., Robinson, J.B., and Bauer, W.D. (2000). Plants secrete substances that mimic bacterial N-acyl homoserine lactone signal activities and affect population density-dependent behaviors in associated bacteria. Mol. Plant Microbe Interact. *13*, 637–648.
5. Dong, Y.H., Xu, J.L., Li, X.Z., and Zhang, L.H. (2000). AiiA, an enzyme that inactivates the acylhomoserine lactone quorum-sensing signal and attenuates the virulence of *Erwinia carotovora*. Proc. Natl. Acad. Sci. USA *97*, 3526–3531.
6. Bassler, B.L., Wright, M., Showalter, R.E., and Silverman, M.R. (1993). Intercellular signalling in *Vibrio harveyi*: sequence and function of genes regulating expression of luminescence. Mol. Microbiol. *9*, 773–786.
7. Hanzelka, B.L., Parsek, M.R., Val, D.L., Dunlap, P.V., Cronan, J.E., Jr., and Greenberg, E.P. (1999). Acylhomoserine lactone synthase activity of the *Vibrio fischeri* AinS protein. J. Bacteriol. *181*, 5766–5770.
8. Laue, B.E., et al., and Williams, P. (2000). The biocontrol strain *Pseudomonas fluorescens* F113 produces the rhizobium small bacteriocin, N-(3-hydroxy-7-cis-tetradecenoyl)homoserine lactone, via HdtS, a putative novel N-acylhomoserine lactone synthase. Microbiology *146*, 2469–2480.
9. Surette, M.G., and Bassler, B.L. (1999). Regulation of autoinducer production in *Salmonella typhimurium*. Mol. Microbiol. *31*, 585–595.
10. Surette, M.G., and Bassler, B.L. (1998). Quorum sensing in *Escherichia coli* and *Salmonella typhimurium*. Proc. Natl. Acad. Sci. USA *95*, 7046–7050.
11. Dry, S., McCarthy, S., and Harris, T. (2000). Structural genomics in the biotechnology sector. Nat. Struct. Biol. *7*, 946–949.
12. Weeks, C.M., and Miller, R. (1999). Optimizing Shake-and-Bake for proteins. Acta Crystallogr. D Biol. Crystallogr. *55*, 492–500.
13. de La Fortelle, E., and Bricogne, G. (1997). Maximum-likelihood heavy-atom parameter refinement for multiple isomorphous replacement and multiwavelength anomalous diffraction methods. In Macromolecular Crystallography, Part A, C.W.J. Carter, and R.M. Sweet, eds. (New York: Academic Press), pp. 472–494,
14. Abrahams, J.P., and Leslie, A.G.W. (1996). Methods used in the structural determination of bovine mitochondrial F1 ATPase. Acta Crystallogr. D Biol. Crystallogr. *52*, 30–42.
15. Kissinger, C.R., Gehlhaar, D.K., and Fogel, D.B. (1999). Rapid automated molecular replacement by evolutionary search. Acta Crystallogr. D Biol. Crystallogr. *55*, 484–491.
16. Holm, L., and Sander, C. (1993). Protein structure comparison by alignment of distance matrices. J. Mol. Biol *233*, 123–138.
17. Iwata, S., et al., and Jap, B.K. (1998). Complete structure of

the 11-subunit bovine mitochondrial cytochrome bc1 complex. Science *281*, 64–71.
18. Ferre-D'Amare, A.R., and Burley, S.K. (1997). Dynamic light scattering in evaluating crystallizability of macromolecules. In Macromolecular Crystallography, Part A, C.W.J. Carter and R.M. Sweet, eds. (New York: Academic Press), pp. 157–166.
19. Lipscomb, W.N., and Strater, N. (1996). Recent advances in zinc enzymology. Chemical Rev. *96*, 2375–2433.
20. Sankaranarayanan, R., et al., and Moras, D. (1999). The structure of threonyl-tRNA synthetase-tRNA(Thr) complex enlightens its repressor activity and reveals an essential zinc ion in the active site. Cell *97*, 371–381.
21. Dock-Bregeon, A., et al., and Moras, D. (2000). Transfer RNA-mediated editing in threonyl-tRNA synthetase. The class II solution to the double discrimination problem. Cell *103*, 877–884.
22. Sauder, J.M., Arthur, J.W., and Dunbrack, R.L., Jr. (2000). Large-scale comparison of protein sequence alignment algorithms with structure alignments. Proteins *40*, 6–22.
23. Miller, C.H., and Duerre, J.A. (1968). S-ribosylhomocysteine cleavage enzyme from *Escherichia coli*. J. Biol. Chem. *243*, 92–97.
24. Otwinowski, A., and Minor, W. (1997). Processing of X-ray diffraction data collected in oscillation mode. In Macromolecular Crystallography, Part A, C.W.J. Carter and R.M. Sweet, eds. (New York: Academic Press), pp. 307–326.
25. Jones, T.A., and Kjeldgaard, M. (1997). Electron-density map interpretation. In Macromolecular Crystallography, Part B, C.W.J. Carter, and R.M. Sweet, eds. (New York: Academic Press), pp. 173–208.
26. McRee, D.E. (1999). XtalView/Xfit-a versatile program for manipulating atomic coordinates and electron density. J. Struct. Biol. *125*, 156–165.
27. Brunger, A.T., et al., and Warren, G.L. (1998). Crystallography & NMR system: A new software suite for macromolecular structure determination. Acta Crystallogr. D Biol. Crystallogr. *54*, 905–921.
28. Christopher, J.A. (1998). SPOCK: The Structural Properties Observation and Calculation Kit (Program Manual) (College Station, Texas: Texas A & M University).

Accession Numbers

Coordinates for Hp_LuxS, Hi_LuxS, Dr_LuxS ($P2_1$), and Dr_LuxS (C2) have been deposited in the Protein Data Bank with accession codes 1J6X, 1J6W, 1INN, and 1J6V, respectively.